Physica E 53 (2013) 36–40

Contents lists available at SciVerse ScienceDirect

Physica E

journal homepage: www.elsevier.com/locate/physe

Effect of substrate temperature on conductivity and microstructures of boron-doped silicon nanocrystals in SiC_x thin films

Qiang Cheng [a], Yuheng Zeng [a], Junjun Huang [a], Ning Dai [a,b], Ye Yang [a], Ruiqin Tan [c], Xingbo Liang [d], Weijie Song [a,*]

[a] Ningbo Institute of Material Technology and Engineering, Chinese Academy of Sciences, Ningbo 315201, PR China
[b] National Laboratory for Infrared Physics, Shanghai Institute of Technical Physics, Chinese Academy of Sciences, Shanghai 200083, PR China
[c] Faculty of Information Science and Engineering, Ningbo University, Ningbo 315211, PR China
[d] Ningbo QL Electricals Co., Ltd. Ningbo 315800, PR China

HIGHLIGHTS

- SiC-matrix p-type Si-NCs were doped through the heavily B-doped CZ-Si target.
- Conductivity increased by 10–100 times when T_s was 200 °C.
- Crystalline fraction increased by ~5% when T_s was 200 °C.
- *fcc* Si-NCs formed in the surface layer when T_s was 200 °C.

GRAPHICAL ABSTRACT

When T_s was ~200 °C, crystalline fraction and conductivity of thin films increased, and *fcc* Si-NCs were formed in the surface layer.

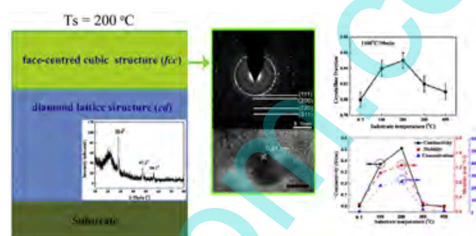

ARTICLE INFO

Article history:
Received 31 December 2012
Received in revised form
18 March 2013
Accepted 7 April 2013
Available online 26 April 2013

Keywords:
Boron doped silicon nanocrystal
Substrate temperature
Face-centered cubic (*fcc*)

ABSTRACT

Boron (B)-doped silicon-rich SiC (SiC_x, $0<x<1$) thin films were deposited using magnetron sputtering (MS) and annealed in a tube furnace. The effect of substrate temperature (T_s) on the conductivity and microstructures of the annealed B-doped SiC_x thin films were studied. The crystalline fraction increased by 5%, while the conductivity increased by 10–100 times, in the annealed thin films deposited at about 200 °C, comparing to that deposited at RT −400 °C. The face-centered cubic (*fcc*) Si nanocrystals (Si-NCs) formed in the surface layer when T_s was about 200 °C. It was suggested that T_s influenced the crystallization, conductivity and even the microstructures of Si-NCs. The proper T_s was helpful to improve the crystallization and conductivity of the B-doped Si-NCs in SiC_x thin film.

© 2013 Elsevier B.V. All rights reserved.

www.spm.com.cn

1. Introduction

Silicon nanocrystals (Si-NCs) in Si–rich SiC (SiC_x, $0<x<1$) matrix have recently been interesting in photovoltaic [1] due to their inherent advantages (adjustable band gaps [2], strong multiple-exciton generation [3] and controllable array-growth structures [4] and low barrier of carrier transport [5]) for developing the next-generation solar cells [6–8]. Also, C coating may be good for the photovoltaic application of Si NCs [9,10]. The formation of Si-NCs in SiC_x thin films usually includes two processes: the phase separation of amorphous silicon and the crystallization of amorphous silicon. Such processes are influenced by the composition and microstructure of the as-deposited thin films [11]. The composition and microstructure of as-deposited thin films will be influenced by the substrate temperature (T_s) during deposition [12]. Till now, many groups have studied Si-NCs in SiC_x thin films and have reported much valuable experimental studies about the formation of Si-NCs [13,14]. However, to our knowledge, the effect of T_s on the formation of Si-NCs in SiC_x thin films are scarcely investigated and remain unclear.

In this work, we deposited the boron (B)-doped SiC_x thin films using different T_s and studied the effect of T_s on the crystallization,

* Corresponding author. Tel./fax: +86 574 86686346.
E-mail address: weijiesong@nimte.ac.cn (W. Song).

1386-9477/$ - see front matter © 2013 Elsevier B.V. All rights reserved.
http://dx.doi.org/10.1016/j.physe.2013.04.006

conductivity and microstructures of the annealed SiC_x thin films. The as-deposited and annealed thin films were studied using Raman measurement, grazing incidence X-ray diffraction (GI-XRD), transmission electron microscopy (TEM), Hall measurements and atomic force microscopy (AFM). It was observed that the crystalline fraction of the annealed B-doped SiC_x thin films was highest when T_s was about 200 °C. Here, the annealed B-doped SiC_x thin films can be also named as SiC_x-matrix B-doped Si-NC thin films, since the Si-NCs formed in the annealed thin films. The face-centered cubic (*fcc*) Si-NCs formed in the surface layer of the annealed SiC_x thin films when T_s was about 100–200 °C. The above results were probably related to the effect of T_s on the compositions of the as-deposited B-doped SiC_x thin films. The underlying mechanism was discussed.

2. Experimental

Quartz plates were used as the substrates, which were cleaned by standard wet chemical process. The B-doped SiC_x ($0<x<1$) thin films were deposited using magnetron co-sputtering (J-sputter8000 magnetron sputtering system) of intrinsic polycrystalline SiC (4 N) and heavily B-doped Czochralski silicon (6 N). The resistivity of heavily B-doped Czochralski silicon was about 1.0×10^{-3} Ω cm; this resistivity corresponded to a B concentration of ~1.17×10^{20} cm^{-3} [15]. The sputtering powers were 220 and 120 W for the Si target and SiC target, respectively. The SiC_x thin films were deposited for 90 min by using Ar as the carrier gas. During deposition, T_s of the substrates range from room temperature (RT, ~20–40 °C) to 400 °C. After deposition the SiC_x thin films were annealed in a tube furnace at 1100 °C for 10 min [13,14,16,17].

The thin films were about 550–600 nm thick, as determined by a profilometer (Veeco Dektak 150). Chemical composition of the SiC_x thin films might be approximately denoted by $Si_{0.75}C_{0.25}$, according to X-ray photoelectron spectroscopy (XPS, Kratos AXIS ULTRA^{DLD}). The thin films were characterized by using a confocal micro-Raman spectroscope (Renishaw inVia) with the excitation of a Nd:YAG laser (532 nm). Grazing incidence X-ray diffraction (GI-XRD, Bruker AXS, D8 Discover, a voltage of 45 kV and a current of 40 mA, Cu K_α radiation $\lambda=1.540562$ Å) was employed to measure the annealed thin films at the incidence angle of 1.5°. A transmission electron microscopy (TEM) (Tecnai F20) was used to study the microstructures of the annealed thin films. The conductivity of the annealed thin films was determined by Hall measurements (Nanometrics HL5500PC). The surfaces of the as-deposited thin films were examined with an atomic force microscopy (AFM, CSPM5500 Scanning Probe Microscopy).

3. Results and discussion

The high-temperature annealing at 1100 °C leads to the crystallization of Si phase in SiC_x thin films [18–20]. The crystalline fraction of Si phase is derived from the Raman spectrum according to the accepted methods [21,22]. In general, the peak of Si phase is fitted using three peaks: 480 cm^{-1} (amorphous silicon), 510 cm^{-1} (nanocrystal silicon), and 520 cm^{-1} (crystal silicon) [21,22]. However, as shown in Fig. 1(a), the peak position of Raman TO-mode shifts to lower wave-numbers (~515 cm^{-1}) for the crystalline Si film herein. The shift of peak position is probably due to a large tensile strain [23] or small grain size [24] in the nanocrystal-Si film. Raman spectra are analyzed with the software of XPSPEAK (version 4.1), which is developed for the division and fitting of peaks. The crystalline fraction of silicon is given by $(I_{c\text{-}Si}+I_{nc\text{-}Si})/(I_{c\text{-}Si}+I_{nc\text{-}Si}+\sigma I_{\alpha\text{-}Si})$, where σ is Raman emission cross-section ratio, $I_{c\text{-}Si}$, $I_{nc\text{-}Si}$ and $I_{\alpha\text{-}Si}$ are the intensities of crystalline silicon, nanocrystal silicon and amorphous silicon. Fig. 1(a) shows the Raman peak of Si phase and its fitting lines in the annealed SiC_x thin film deposited at 200 °C. The dotted line denotes the experimental data. The solid lines result from fitting. Fig. 1(b) shows the crystalline fractions of the annealed SiC_x thin films deposited in the temperature range from RT to 400 °C. The crystalline fraction first increases and then decreases with the increase of T_s. The crystalline fraction reaches the highest value (~85%) when T_s is 200 °C.

Fig. 2(a) shows the conductivity, carrier concentration and carrier mobility of the annealed SiC_x thin films deposited in the temperature range from RT to 400 °C. Similar to the change of crystalline fraction, the conductivity of the annealed SiC_x thin films first increases and then decreases with the increase of T_s. The conductivity reaches its highest value (0.51 S/cm) when T_s is 200 °C, whereas it decreases when T_s is more than 200 °C. The highest conductivity is about 10–100 times higher than the lowest one. In addition, Fig. 2(a) shows the carrier mobility and carrier concentration of the annealed SiC_x thin films deposited in the temperature range from RT to 400 °C. The carrier mobility and carrier concentration both increase first and then decrease with the increase of T_s. They both reach the highest value when T_s is 200 °C. The carrier mobility is in the range from 0.2 to 1.2 $cm^2\,V^{-1}\,s^{-1}$. The carrier concentration is in the range from 0.1×10^{18} to 2.5×10^{18} cm^{-3}. The changes of carrier mobility and carrier concentration are similar to that of conductivity. The conductivity of the annealed SiC_x thin films at the temperatures from −20 to 120 °C is

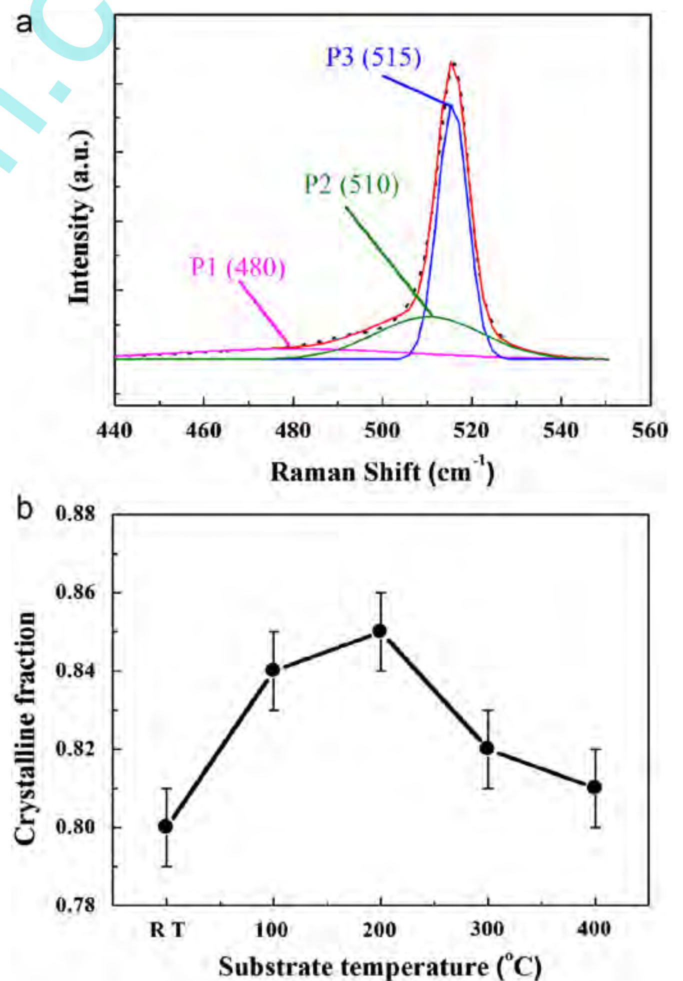

Fig. 1. (a) Raman peak of Si phase and its fitting lines in the annealed SiC_x thin film deposited at 200 °C and (b) the crystalline fractions of Si phase in the annealed SiC_x thin films deposited in the temperature range from RT to 400 °C (1100 °C/10 min).

www.spm.com.cn

determined by Hall measurements. The activate energy of conductivity (E_a) is extracted from the dependence of conductivity on temperature. Fig. 2(b) shows E_a in the annealed SiC_x thin films deposited at different T_s. E_a reaches its lowest value when T_s is 200 °C. The above results suggested that T_s could significantly change the conductivity and E_a of the annealed SiC_x thin films. It should be mentioned that although B doping is an important issue, it is not discussed here. Since to determine directly the dopant location and efficiency by experiments is tremendously challenging in the nanometer-sized regime. The details of B doping can be refereed in the theoretical calculations [25–28].

The effect of T_s on the crystallization and conductivity of the annealed SiC_x thin films are discussed as following. It is known that T_s can provide the energy for the sputtering atoms during deposition. On one hand, increasing T_s can facilitate the Si–Si bonds and then the formation of crystalline Si clusters, which will act as the nuclei of Si-NCs and enhance the formation of Si-NCs. On the other hand, increasing T_s will also facilitate the formation of Si–C bonds [29–31]. Since the bonding energy of Si is higher in Si–C network than in Si–Si network [32], the diffusion barriers of Si should be higher in Si–C network than in Si–Si one. Hence, the formation of Si–C bonds in the as-deposited thin film would suppress the diffusion of Si and also suppress the crystallization of Si phase. The above analysis suggested that there was a proper range of substrate temperature which was useful to enhance the crystallization of SiC_x thin films. T_s at about 100–200 °C is useful for the crystallization of the SiC_x thin films.

Fig. 3 shows the GI-XRD spectrum of the annealed SiC_x thin film deposited at 200 °C. The three most strong peaks of the GI-XRD spectrum are located at 28.4°, 47.3° and 56.1°. According to the standard Joint Committee on Powder Diffraction Standard (JCPDS) cards, these peaks originate from the cubic-diamond (*cd*) silicon crystal. The *cd* Si has a lattice constant of 0.543 nm, in agreement with previous reports [33,34].

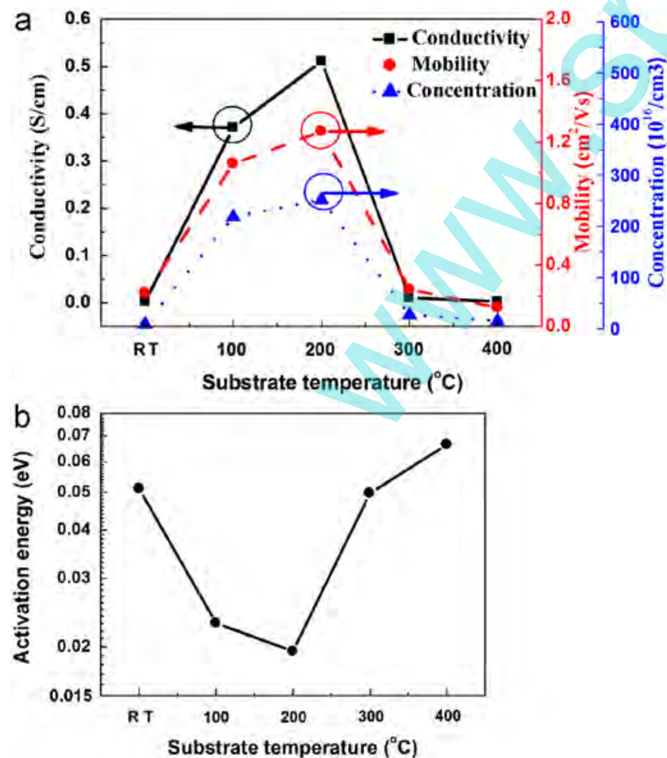

Fig. 2. (a) Conductivity, carrier concentration, carrier mobility, and (b) activation energy of the annealed SiC_x thin films deposited in the temperature range from RT to 400 °C.

Fig. 4(a) and (b) show the high-resolution (HR) TEM images and the selected area electron diffraction (SAED) pattern of the surface layer of the thin film. The lattice spacing of the Si crystal is about

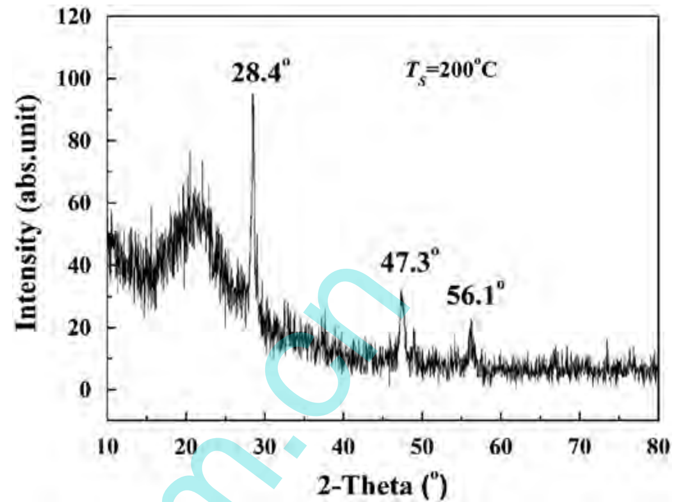

Fig. 3. GI-XRD spectrum of the annealed SiC_x thin film deposited at 200 °C.

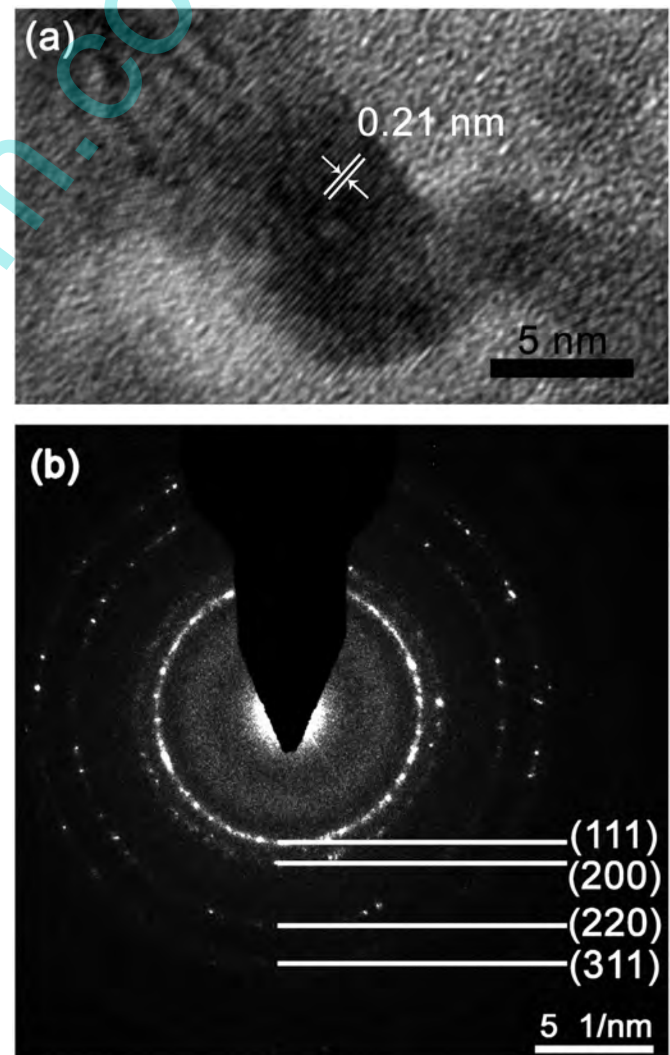

Fig. 4. (a) show the high-resolution (HR) TEM image and (b) the selected area electron diffraction (SAED) pattern of the annealed thin film deposited at 200 °C.

www.spm.com.cn

Table 1
R, R^2, reduction of R^2, the corresponding lattice spacing and miller index of the surface layer of the annealed thin film deposited at 200 °C.

No.	R (1/nm)	R^2 (1/nm^2)	Reduction of R^2	Lattice spacing (nm)	*hkl*
1	4.742	22.49	3	0.2109	111
2	5.456	29.77	4.0	0.1833	200
3	7.849	61.61	8.2	0.1274	220
4	9.184	84.34	11.2	0.1089	311

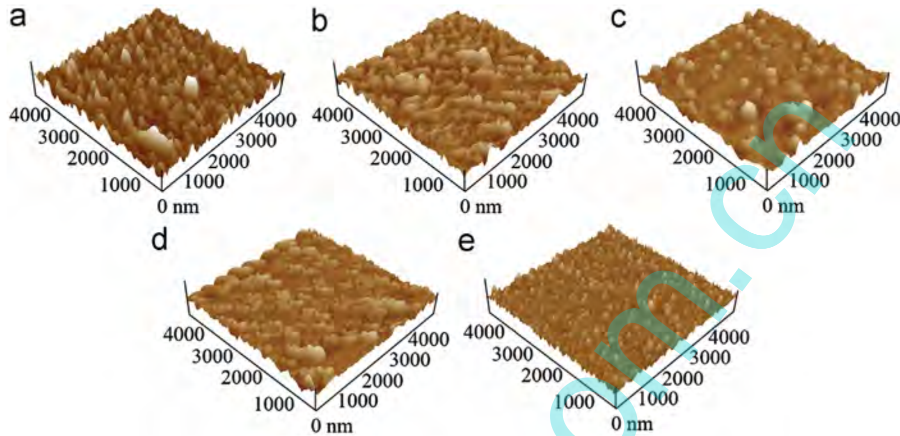

Fig. 5. AFM images of the surface morphology in the as-deposited SiC_x thin films, (a) RT, (b) 100 °C, (c) 200 °C, (d) 300 °C, and (e) 400 °C.

0.21 nm, smaller than the (1 1 1)-plane spacing of *cd*-Si crystal (0.314 nm). SAED pattern is used to identify the structure of Si crystals. The radius of electron diffraction rings (R), R^2, the reduction of R^2, lattice spacing and miller index are listed in Table 1. The reduction of R^2, approximately following the ratio of 3:4:8:11, corresponds to that of the *fcc* crystals. The results of HR-TEM and SEAD suggest that the Si-NCs in the surface layer are in the *fcc* structure. The surface layers of the annealed SiC_x thin films deposited at RT, 100, 300 and 400 °C were also characterized by HR-TEM and SAED. Only the thin film deposited at 100 °C has the *fcc* Si-NCs in the surface layer, while the other thin films deposited at RT, 300 or 400 °C do not have the *fcc* Si-NCs. The above TEM results indicated that T_s would probably influence the structure of Si-NCs in the surface of the thin films.

There are several papers reporting the formation of *fcc* Si-NCs [35–38]. In these papers, the formation of *fcc* Si-NCs is generally attributed to high energy, high temperature, and high nano-induced pressure [35–40]. Our recent work also indicates that *fcc* Si-NCs are readily formed in the surface layer of high-temperature annealed SiC_x thin films [41]. In terms of thermodynamics, we suggested that the formation of *fcc* Si-NCs is induced by the significant additional nano-induced pressure and the low surface free energy [41].

We now discuss the effect of T_s on the formation of *fcc* Si-NCs. First, the effect of surface morphology is studied. Fig. 5 shows the AFM images of the surface morphologies in the as-deposited SiC_x thin films. The features of the AFM images and relative statistical data show no significant differences among the thin films deposited in the temperature range from RT to 400 °C. It is suggested that the generation of *fcc* Si-NCs is hardly influenced by the surface morphology. Second, the effect of compositions of the as-deposited thin films are studied. The previous analysis suggested that the Si–Si network was preferentially formed when T_s was 200 °C. Comparing to the bond length of Si–C, the bond length of Si–Si is more close to the bond length of Si–Si in Si-NCs, the lattice mismatch of Si-NC surface should be smaller in Si–Si network. Thus, the Si–Si network is probably more favored to reduce the surface free energy of Si-NC nuclei and the formation of *fcc* Si-NCs. The reason that *fcc* Si-NCs are preferentially generated in the SiC_x thin films deposited at ~200 °C is still unclear, but it is possibly related to the compositions of the as-deposited SiC_x thin films. A further study is still necessary to classify the issue.

4. Conclusions

The effect of T_s on the conductivity and microstructures of SiC_x-matrix B-doped Si-NCs thin films were studied. The crystalline fraction increased by 5%, while the conductivity increased by 10–100 times, in the annealed thin film deposited at about 200 °C, comparing to that deposited at RT-400 °C. It was suggested that the proper T_s was helpful to improve the crystallization and conductivity of the boron-doped Si-NC thin films. In addition, the annealed thin film deposited at ~200 °C usually had the *fcc* Si-NCs in the surface layer. The preferential generation of *fcc* Si-NCs was possibly related to the compositions of the as-deposited SiC_x thin films.

Acknowledgement

The authors would like to thank the financial supports by Natural Science Foundation of China for Young (Grant No. 61106096), China Postdoctoral Science Foundation (Grant Nos. 2012T50535 and 20110491831), Natural Science Foundation of Ningbo (Grant No. Y10820UA32), and aided program for Science and Technology Innovative Research Team of Ningbo Municipality (Grant No. 2009B21005).

References

[1] E.C. Cho, M.A. Green, G. Conibeer, D. Song, Y.H. Cho, G. Scardera, S. Huang, S. Park, X.J. Hao, Y. Huang, L. Van Dao, Advances in OptoElectronics, 2007 (2007) 69578/69571-69578/69511.
[2] C. Delerue, M. Lannoo, G. Allan, Physical Review Letters 84 (2000) 2457.

www.spm.com.cn

[3] M.C. Beard, K.P. Knutsen, P. Yu, J.M. Luther, Q. Song, W.K. Metzger, R.J. Ellingson, A.J. Nozik, Nano Letters 7 (2007) 2506.
[4] J. Heitmann, F. Müller, M. Zacharias, U.G. sele, Advanced Materials 17 (2005) 795.
[5] M. Green, E. Cho, Y. Cho, E. Pink, T. Trupke, K. Lin, T. Fangsuwannarak, T. Puzzer, G. Conibeer, R. Corkish, All-silicon tandem cells based on 'artificial'semiconductor synthesised using silicon quantum dots in a dielectric matrix, in: Proceedings of the 20th European Photovoltaic Solar Energy Conference and Exhibition, 2005, pp. 3.
[6] M.A. Green, "Third generation" photovoltaics and silicon nanostructures, in: 2008 Fifth IEEE International Conference on Group IV Photonics, 2008, pp. 389–389.
[7] G. Conibeer, Materials Today 10 (2007) 42.
[8] L. Pavesi, R. Turan, Silicon nanocrystals: fundamentals, Synthesis and Applications, Wiley-VCH, 2010.
[9] L.L. Kazmerski, Journal of Electron Spectroscopy and Related Phenomena 150 (2006) 105.
[10] Z. Ni, X. Pi, D. Yang, RSC Advances 2 (2012) 11227.
[11] Y. Liu, T. Chen, Y. Fu, M. Tse, J. Hsieh, P. Ho, Y. Liu, Journal of Physics D: Applied Physics 36 (2003) L97.
[12] J. Huang, Y. Zeng, R. Tan, W. Wang, Y. Yang, N. Dai, W. Song, Applied Surface Science 270 (2013) 428.
[13] D. Song, E. Cho, Y. Cho, G. Conibeer, Y. Huang, S. Huang, M. Green, Thin Solid Films 516 (2008) 3824.
[14] A.G. Imer, I. Yildiz, R. Turan, Physica E: Low-dimensional Systems and Nanostructures 42 (2010) 2358.
[15] W.R. Thurber, National Bureau of Standards, 1981.
[16] M. Zacharias, P. Streitenberger, Physical Review B: Condensed Matter 62 (2000) 8391.
[17] P. Löper, A. Hartel, M. Künle, D. Hiller, S. Janz, M. Hermle, M. Zacharias, A. Hartel, S.W. Glunz, Silicon quantum dot absorber layers for all-silicon tandem solar cell: optical and electrical characterisation, in: 24th European Photovoltaic Solar Energy Conference and Exhibition, Hamburg, Germany, 2009.
[18] D. Hiller, S. Goetze, M. Zacharias, Journal of Applied Physics 109 (2011) 054308-054308-054305.
[19] S.T.H. Silalahi, Q.V. Vu, H.Y. Yang, K. Pita, Y. Mingbin, Applied Physics A 98 (2010) 867.
[20] Y. Wang, X. Liao, Z. Ma, G. Yue, H. Diao, J. He, G. Kong, Y. Zhao, Z. Li, F. Yun, Applied Surface Science 135 (1998) 205.
[21] E. Vallat-Sauvain, C. Droz, F. Meillaud, J. Bailat, A. Shah, C. Ballif, Journal of Non-Crystalline Solids 352 (2006) 1200.
[22] R. Tsu, J. Gonzalez-Hernandez, S. Chao, S. Lee, K. Tanaka, Applied Physics Letters 40 (1982) 534.
[23] I. De Wolf, J. Vanhellemont, A. Romano-Rodriguez, H. Norstrom, H.E. Maes, Journal of Applied Physics 71 (1992) 898.
[24] S. Veprek, F.A. Sarott, Z. Iqbal, Physical Review B: Condensed Matter 36 (1987) 3344.
[25] M. Fujii, S. Hayashi, K. Yamamoto, Journal of Applied Physics 83 (1998) 7953–7957.
[26] X.D. Pi, R. Gresback, R.W. Liptak, S.A. Campbell, U. Kortshagen, Applied Physics Letters 92 (2008) 123102.
[27] G. Cantele, E. Degoli, E. Luppi, R. Magri, D. Ninno, G. Iadonisi, S. Ossicini, Physical Review B: Condensed Matter 72 (2005) 113303.
[28] X. Pi, X. Chen, D. Yang, Journal of Physical Chemistry C 115 (2011) 9838–9843.
[29] H. Shaik, K. Thulasiraman, G.M. Rao, Applied Surface Science 258 (2011) 2989.
[30] H. Colder, R. Rizk, M. Morales, P. Marie, J. Vicens, I. Vickridge, Journal of Applied Physics 98 (2005) 024313-024313-024310.
[31] D. Song, E.C. Cho, G. Conibeer, Y. Huang, C. Flynn, M.A. Green, Journal of Applied Physics 103 (2008) 083544-083544.083547.
[32] Q.Y. Tong, K. Gutjahr, S. Hopfe, U. Gosele, T.H. Lee, Applied Physics Letters 70 (1997) 1390.
[33] G. Viera, S. Huet, M. Mikikian, L. Boufendi, Thin Solid Films 403 (2002) 467.
[34] Q. Cheng, S. Xu, S. Huang, K. Ostrikov, Crystal Growth & Design 9 (2009) 2863.
[35] X.W. Du, W.J. Qin, Y.W. Lu, X. Han, Y.S. Fu, S.L. Hu, Journal of Applied Physics 102 (2007) 013518-013518-013514.
[36] N. Saxena, P. Kumar, A. Agarwal, D. Kanjilal, Physica Status Solidi A Applications and Material Science 209 (2012) 283.
[37] Y.W. Lu, X.W. Du, J. Sun, S.L. Hu, X. Han, H. Li, Applied Physics Letters 90 (2007) 241910-241910-241913.
[38] G. Viera, M. Mikikian, E. Bertran, P.R. i Cabarrocas, L. Boufendi, Journal of Applied Physics 92 (2002) 4684.
[39] a W.L.S. Hu, W. Liu, Y. Dong, S. Cao, J. Yang, Journal of Physics: Condensed Matter 23 (2011) 205302;
b S. Hu, W. Li, W. Liu, Y. Dong, S. Cao, J. Yang, Journal of Physics: Condensed Matter 23 (2011) 205302.
[40] S. Hu, J. Zhang, J. Yang, J. Liu, S. Cao, Applied Physics Letters 99 (2011) 151901-151901-151903.
[41] Y. Zeng, X. Chen, Q. Cheng, J. Zhao, W. Song, N. Dai, Applied Surface Science 265 (2013) 286.

www.spm.com.cn